Research

Assessment of three mixed arrays dataset for subsurface cavities detection using resistivity tomography as inferred from numerical modelling

Wael Dosoky[1]

Abstract

The present study deals with the evaluation of a three-mixed array dataset for the detection of subsurface cavities using conceptual air-filled cavity model sets at different depths. Cavity models were simulated using the forward modelling technique to generate synthetic apparent resistivity data for three common individual arrays. These arrays are dipole–dipole (DD), pole–dipole (PD), and Wenner–Schlumberger (WS). The synthetically apparent resistivity data obtained from two different individual arrays were merged to form a high-resolution single model. Consequently, three possible mixed arrays datasets can be obtained: the dipole–dipole-Wenner–Schlumberger (DD+WS), pole–dipole, and Wenner–Schlumberger (PD+WS), and dipole–dipole and pole–dipole (DD+PD). The synthetically apparent resistivity data for both the individual and mixed arrays were inverted using Res2dinv software based on the robust constrain inversion technique to obtain a 2D resistivity model section. The inverted resistivity sections were evaluated in terms of their recovering ability of the model's parameters (e.g. resistivity, and geometry). The results show that the individual arrays can resolve the location and dimensions of the cavity within reasonable accuracy only at a depth not exceeding 6 m below the surface. On the other hand, a significant resolution enhancement in model resistivity with increasing depth was observed when the mixed arrays were used. The (DD+WS) mixed arrays dataset brings up better model resistivity and shows closer parameters to the true actual model among the other mixed arrays. So it is strongly recommended for cavity detection studies.

Article highlights

- Comparison between three traditional arrays and mixed array datasets in delineation of the geometry of subsurface cavities using numerical simulation was made.
- The resolution of the obtained resistivity model can be enhanced by using mixed array datasets.
- The numerical simulations are considered an effective tool for predicting several scenarios for studying the electrical response of any subsurface structures.

Keywords Mixed arrays · Individual arrays · Numerical modelling · Cavity detection

✉ Wael Dosoky, wael.desoky@sci.svu.edu.eg | [1]Faculty of Science, Geology Department, South Valley University, Qena, Egypt.

1 Introduction

The electrical resistivity tomography (ERT) technique is considered one of the most common non-destructive geophysical tools used for shallow subsurface investigation. It has a wide range of applications, such as hydrological [1–3], environmental [4, 5], Structural mapping [6–8], and geohazard [9, 10] investigations. The ERT technique is a widely used geophysical method for cavities detection [11–13]. However, accurate mapping of subsurface geological structures (e.g. cavities) extremely depends on a proper selection of array for carrying the field ERT survey. There are many different types of electrode arrays used in resistivity surveys [14] but the most commonly used ones are the Wenner (W), Wenner–Schlumberger (WS), dipole–dipole (DD), pole–dipole (PD), pole–pole (PP) arrays [15–17]. Each array has particular merits for imagining a specific geological structure and thus depends on different factors such as depth of investigation, resolution, data coverage, and sensitivity of noise level [18].

Many authors have distinguished and compared the electrode arrays in order to determine their ability to detect different geological features such as cavities, faults, dykes, layers, and so on [19–22]. A lot of these studies depend on a numerical modelling approach which gives insight into the accuracy of the ERT method for resolving different scenarios of geological structures before a real costly field or laboratory investigations are carried out [23, 24]. In this manner, [21] made a comparison between ten electrode arrays using five synthetic models. [25] has studied the response of three different electrode arrays (W, WS, and DD) on resolving conceptual subsurface cavities. [26] investigated the uncertainty of resistivity image survey on the detection of subsurface cavities. All of the above-mention studies reveal that the DD array is the best among the other arrays for cavity surveys. However, one possible limitation of this array it provides a small signal for measurement, and consequently it can yield noisy data [19, 27].

Despite the efficiency of resistivity imagines surveys in many applications, the (ERT) method often shows an exponential decrease in model resolution and recovering ability with increasing the depth of investigation [27]. Decreasing the inter-electrode spacing of an array can increase the resolution. However, using a small electrode spacing will decrease the investigation depth unless more electrodes and cables are utilized [28]. Determining accurate geometry of the subsurface structure using the resistivity technique is still a challenging task [29, 30]. To overcome this problem, two different array datasets can be merged to form one single composite model with high resolution compared to the use of individual array data. The advantages that stand behind using composite datasets are increasing the data point, increasing data levels, and overlapping data levels. Consequently, a better resolution of a particular model can be obtained [29, 31–33].

Therefore, the main goal of the present study is to assess the performance of mixed array datasets technique in cavities detection using a numerical modelling approach in order to define the optimum array data types to be mixed for enhancing the resolution of the obtained resistivity model with increased depth. In this study, a conceptual cavity models located at different depths were simulated using forward modelling for DD, PD, and WS arrays. The synthetically resistivity data of these individual arrays were merged, and therefore three possible combinations of datasets can be obtained. The first one is the dipole–dipole and pole–dipole datasets (DD+PD), the second is pole–dipole and Wenner–Schlumberger (PD+WS), whereas the third one is a combination between dipole–dipole and Wenner–Schlumberger (DD+WS). The resistivity data of both individual and mixed arrays were inverted and displayed in 2D resistivity sections. These sections were evaluated and examined in terms of the resolution and capability in the detection of the cavity models.

2 Methodology

The ERT numerical modelling approach is used to predict the resistivity response of a well-known given model. In the present study, the ERT numerical modelling was used to examine the resistivity imaging accuracy for subsurface cavities resolving using mixed array datasets. The following procedures were achieved through three steps: forward modelling of the synthetic cavity models using three common individual arrays (DD, PD and WS), merging the synthetic data of the selected resistivity arrays. Finally inverse modelling all the synthetic data sets of both individual and mixed arrays to reconstruct the true resistivity distribution of the subsurface. Figure 1 illustrates a typical flow chart of the steps methodology which were employed in the current work. A detailed description of the steps methodology can be presented as follows:

2.1 Forward modelling

In the present study, four synthetic models were created to simulate air-filled cavities in a homogenous limestone as a host medium (Fig. 2). These models are more or less similar to those used by [26]. The model resistivity values were chosen to be 10,000 Ω m for the air-filed cavities and 1000 Ω m for the limestone [12, 34]. The air-filled cavity models

**Fig. 1** Flow chart summarized the methodology steps
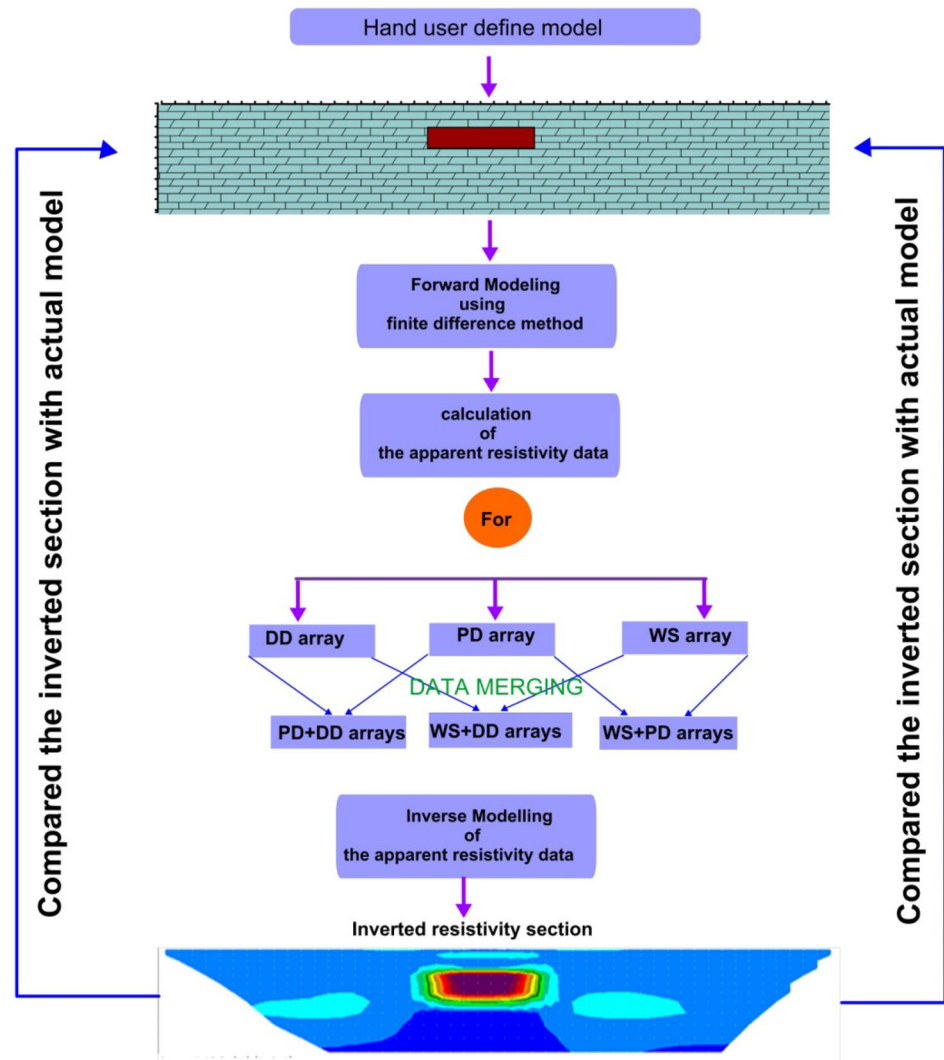
have the same dimensions (16 m length×4 m wide) which are located at different four depth levels coded as L1 (4.5 m), L2 (6.5 m), L3 (8.5 m), and L4 (10.5 m). The synthetic potential differences data for the selected three arrays (DD, PD, and WS) were calculated for each model using the RES-2DMOD software Ver. 3.03.01 [35]. The calculation of the potential differences data is based on the finite difference method [36] which determines the potentials at each node of the rectangular resistivity model discretization mesh. 51 electrodes with a 2 m electrode spacing were used for all the created models.

2.2 Data merging

The performance of a resistivity survey with a different electrode array for a constant profile length yields a different depth of investigations, different number of data points, and different number of data levels. For example, measurements were executed by using dipole–dipole and pole–dipole arrays with inter-electrode spacing equal to 2 m, and the measurements were repeated along the survey line for n values equal to 1, 2, and 3. The number of datum points produced by such measurement will be 141 and 144 for dipole–dipole and pole–dipole arrays respectively. On the other hand, the median depth of investigation for dipole–dipole is about 0.83, 1.394, and 1.924 m for n values of 1, 2, and 3 respectively. While the median depth of investigation for pole–dipole for the same variance of n values are about 1.038, 1.85, and 2.6 [37]. If the data of these two arrays were used, the data sets would have 285 data points and six data levels. This results in a pseudo section with overlapping data levels containing a higher number of data points and data levels, consequently the interpolation between data points can be reduced by reducing the spacing between data levels. In the present study after the calculation of the synthetic apparent resistivity values for cavity models L1, L2, L3, and L4
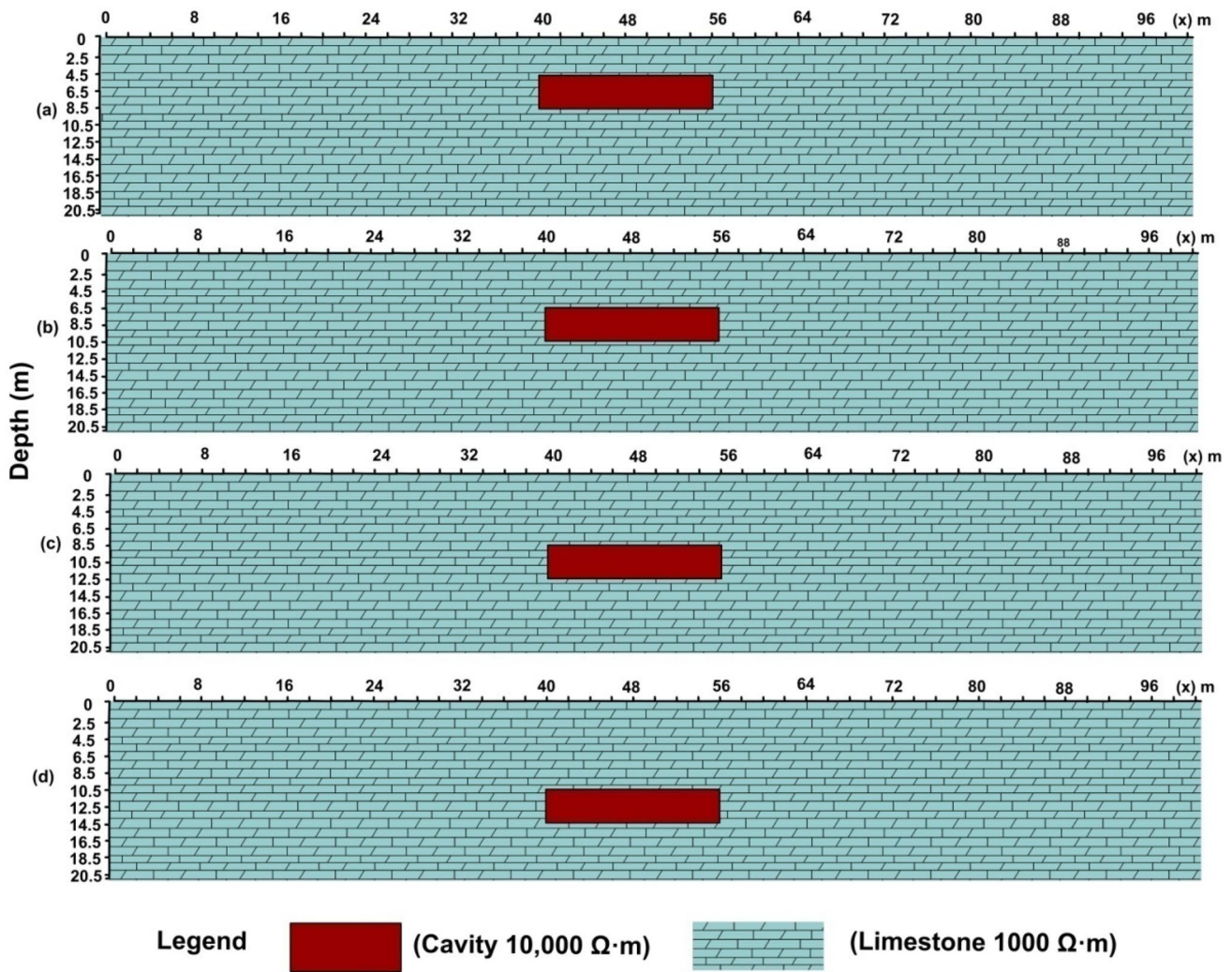
Fig. 2 Resistivity synthetic models simulate an air-filled cavity embedded in limestone rock located at different depth levels **a** L1 cavity (4.5 m), **b** L2 cavity (6.5 m), **c** L3 cavity (8.5), **d** L4 cavity (10.5)

using RES2DMOD software, the obtained data for each individual array type were saved in RES2DINVE ver. 3.54 format. Then a new file in the type of Excel sheet format was generated in order to collect and mix the apparent resistivity data from each of two individual arrays types for cavity models L1, L2, L3, and L4. The apparent resistivity as well as some information like electrode spacing and number of data points were arranged in the mixed data files according to [27]. Finally, the obtained mixed data file were saved into the DAT extension to be read by the RES2DINVE ver. 3.54 software which supports the use of such mixed datasets. The total number of data points and data levels for each individual and composite arrays used in the present study are shown in Table 1. Figure 3 shows the distribution of data points for the WS and PD arrays and their mixed data as a representative example.

2.3 Inverse modelling

The synthetic apparent resistivity datasets were inverted for both the individual array types and the mixed one

Table 1 Number of data points and data levels for both individual and mixed arrays

Array	Number of data points	Number of data levels
DD	1283	45
PD	930	24
WS	978	35
DD-PD	2213	69
DD-WS	2261	80
PD-WS	1908	59
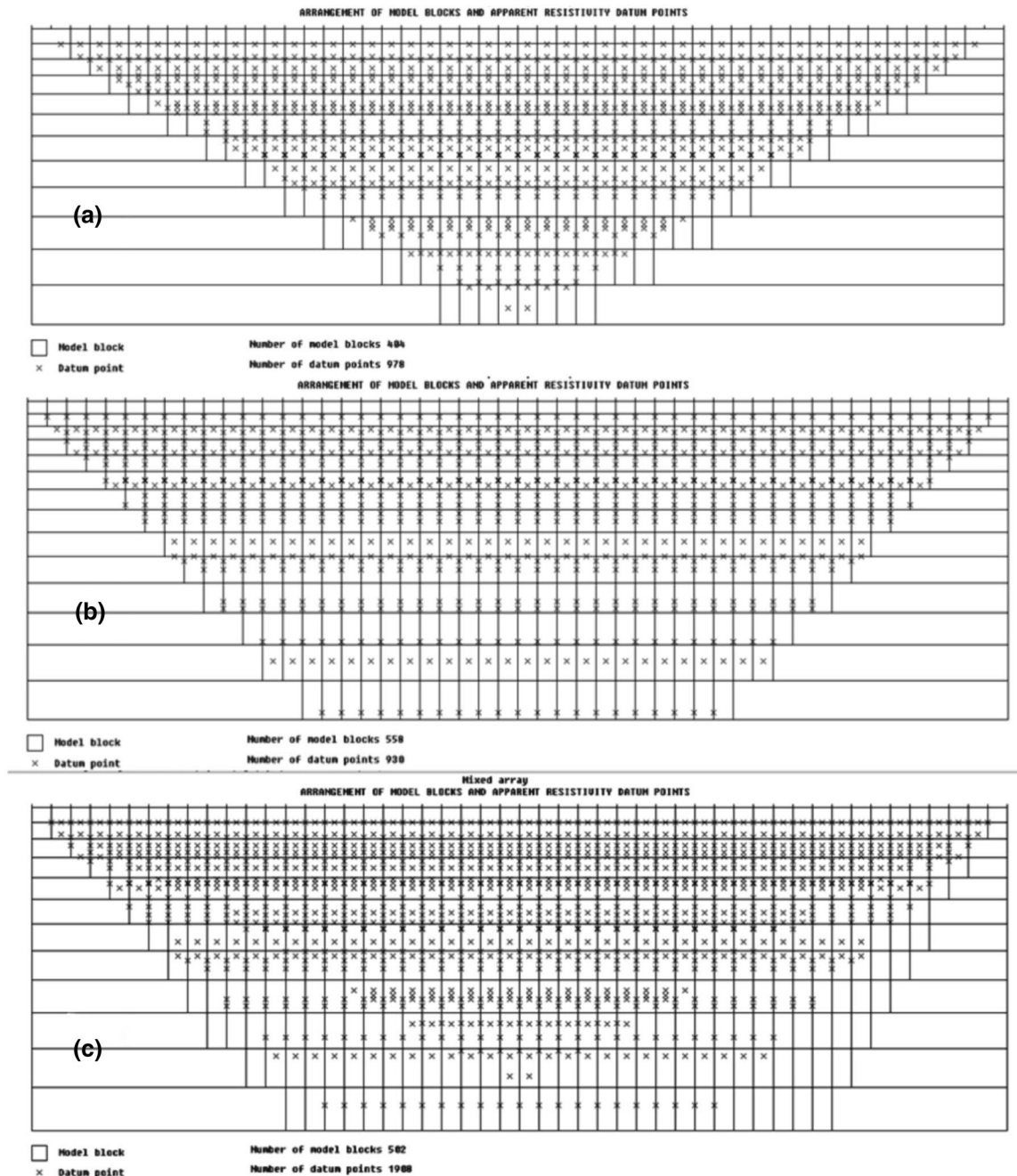
Fig. 3 A representative example of the distribution of data points for **a** WS array, **b** PD array, **c** mixed arrays of (WS+PD)

to obtain model parameters such as the true resistivity distribution of the subsurface. The inversion modelling was carried out using RES2DINV software [27]. The inversion process using this software was accomplished using L1-norm optimization. The L1-norm optimization, otherwise called blocky or robust constrain inversion technique [38]. The robust constraint inversion technique attempts to minimize the absolute difference (Abs.) between the

measured and the calculated apparent resistivity values. It can be a good choice when geological discontinuities are expected since it produces resistivity models characterized by sharp boundaries across the different resistivity layers. The robust inversion routine was chosen to carry out the inverse modelling process for all data to avoid the smearing effect on the boundaries [38]. Table 2 displays the parameters used for the inversion process.
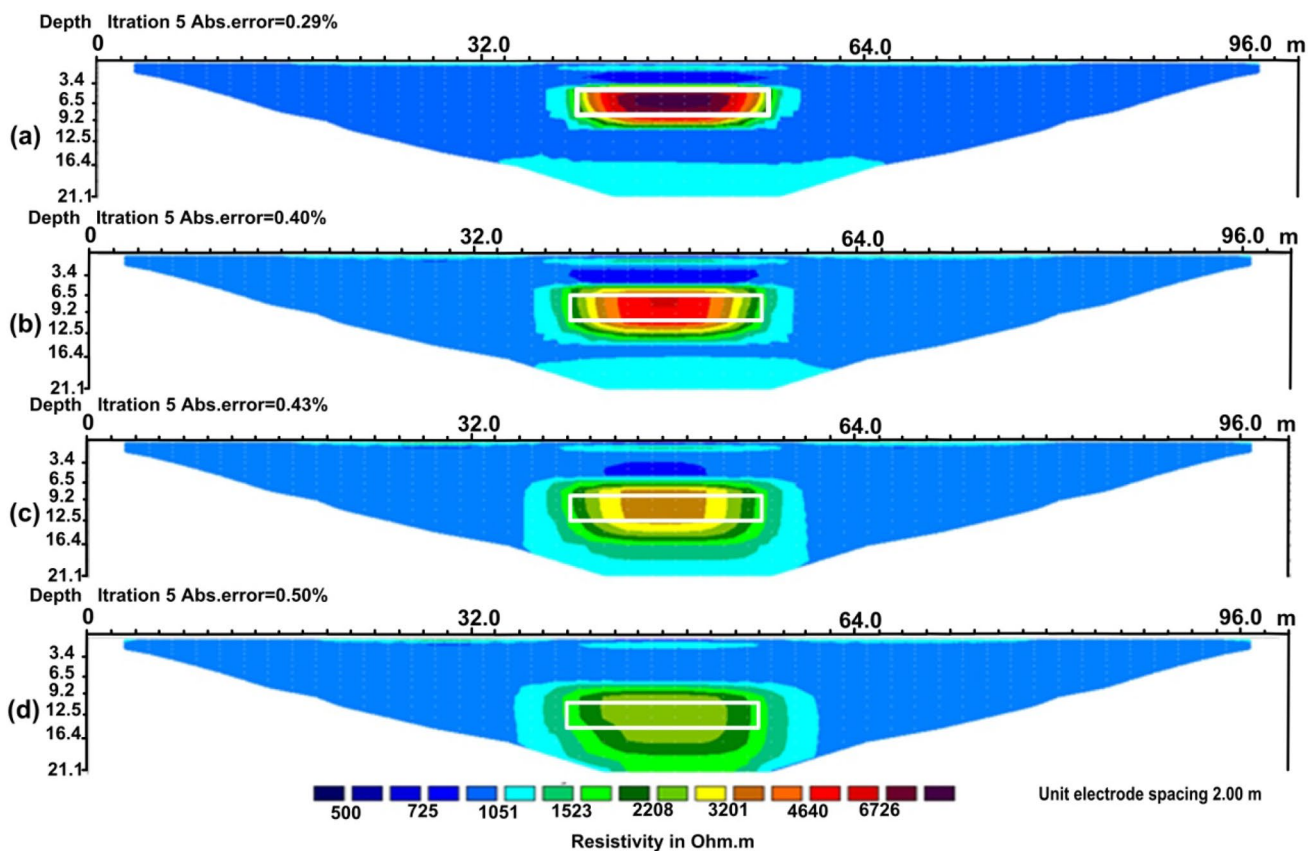
3 Results

The inverted sections obtained from the inversion process for the three selected individual arrays are shown in Figs. 4 and 5, and Fig. 6 for DD, PD, and WS respectively. For a

Table 2 The used parameters during the inversion process

Inversion parameters	Values
Initial damping factor	0.25
Minimum damping factor	0.015
Number of iterations	5
Increase of the damping factor with depth	1.05
Robust data inversion constraint is used with the cut off factor	0.05
Robust model inversion constraint is used with the cut off factor	0.005
Number of nodes between adjacent electrodes	4
Extended model	Used
Reduce the effect of side blocks	None
Type of mesh	Normal

better comparison, the same color scale of all the inverted sections was used. These figures reflect that all the above-mention arrays can resolve the cavity models more efficiently for the shallower depth level than the deeper one and the resolution of the inverted image decrease as the cavity depth increase because the measurement sensitivity decreases with survey depth [18]. The cavity model (L1) located at 4.5 m depth (Fig. 2a) was well recovered by the DD, PD, and WS arrays, as shown in Figs. 4a and 5a, and 6a. The top boundary of the cavity anomaly has coincided with the actual cavity model location however, the bottom boundary is misplaced and extended down the actual cavity model. The cavity model (L2) located at 6.5 m depth (Fig. 2b) was resolved by the three array types as a high resistivity anomaly zone surrounded by a lower resistivity background with a noticeable exaggeration in the anomaly size compared with the actual cavity model location and size (Figs. 4b and 5b, and 6b). There is a misplaced of the top and bottom boundaries of a model anomaly in the range of 1–2.5 m. The inverted resistivity sections for the cavity model (L3) were poorly resolved by all the selected three individual arrays (Figs. 4c and 5c, and 6c). The cavity anomalies zone were highly exaggerated in their size
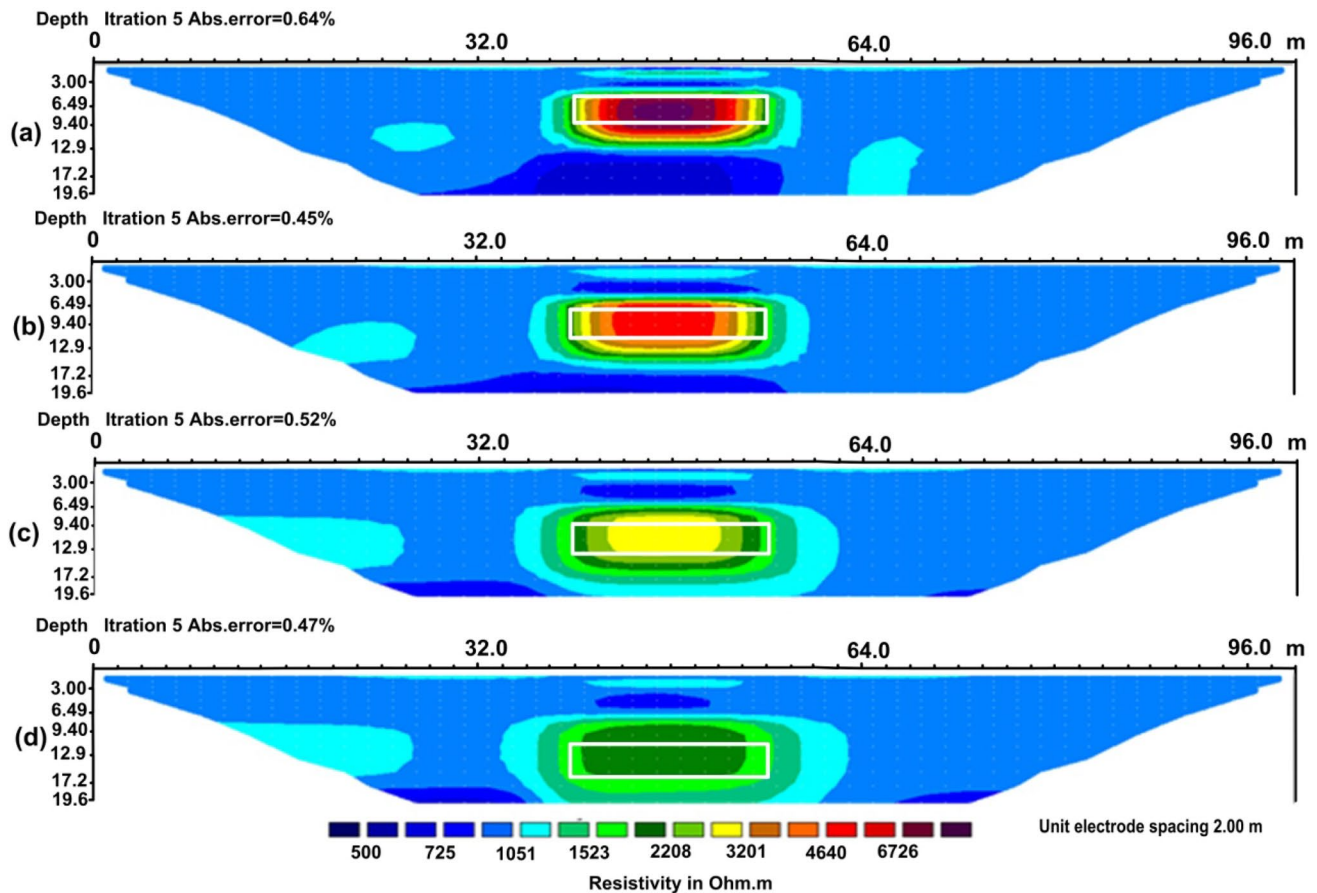

Fig. 4 The inverted resistivity models using DD array for the cavity models: **a** L1, **b** L2, **c** L3, **d** L4. The white boxes represent the actual position and dimensions of the modelled cavities

Fig. 5 The inverted resistivity models using PD array for the cavity models: **a** L1, **b** L2, **c** L3, **d** L4. The white boxes represent the actual position and dimensions of the modelled cavities

compared with the actual cavity model location and size. At a depth of 10.5 m the cavity models (L4) recovered poorly by both the DD and PD arrays, where the bottom of the resistivity anomaly zone extended down to the end of the inverted sections depth and the top boundaries of cavity anomaly misplaced by 2–4 m compared with the actual location of the modelled cavity (Figs. 4d and 5d,). On the other hand, the inverted resistivity section with the WS array (Fig. 6d) failed to reconstruct the deep cavity model.

By comparing the inverted resistivity anomaly of the modelled cavities obtained by the individual arrays with the true resistivity of the actual model as illustrated in Table 3, it is observed that the DD array reconstructed the cavity's resistivity better than PD and WS arrays.

The mixed array datasets of DD-WS (Fig. 7) show the best resolution inverted image for the cavity models compared with DD-PD and PD-WS composite datasets, where the actual shape and location for most of the cavity models are accurately resolved. Figure 7a and b show a good match between the inverted anomalies' location and shape with the true cavity models, where the top surface of inverted anomalies coincides with the actual

top boundary of the actual cavity model, and the bottom boundary of the anomalies was overestimated only with 1 m relative to the true location of the actual cavity. The inverted resistivity model for the intermediate cavity (L3) located at 8.5 m depth (Fig. 7c) shows a good correlation with the actual model. The top and bottom resistivity anomaly was overestimated by about 1.3 m compared to the actual cavity location.

Comparing the inverted resistivity model of composite datasets of DD-WS for the intermediate cavity (L3) with inverted resistivity sections of the DD and WS arrays (Figs. 4c and 6c) one can notice that, the anomaly cavity obtained by DD and WS is highly exaggerated and there are a misplaced of the top and bottom anomaly boundaries between 3 and 6 m. On the other hand, the inverted resistivity anomaly for the intermediate cavity (L3) shows maximum values of 3853 Ω m, 2208 Ω m, and 6726 Ω m obtained by DD, WS, and composite DD-WS datasets respectively. Although the true resistivity of the cavity model is 10,000 Ω m, the composite DD-WS datasets show a closer inverted resistivity value to the true model's resistivity.
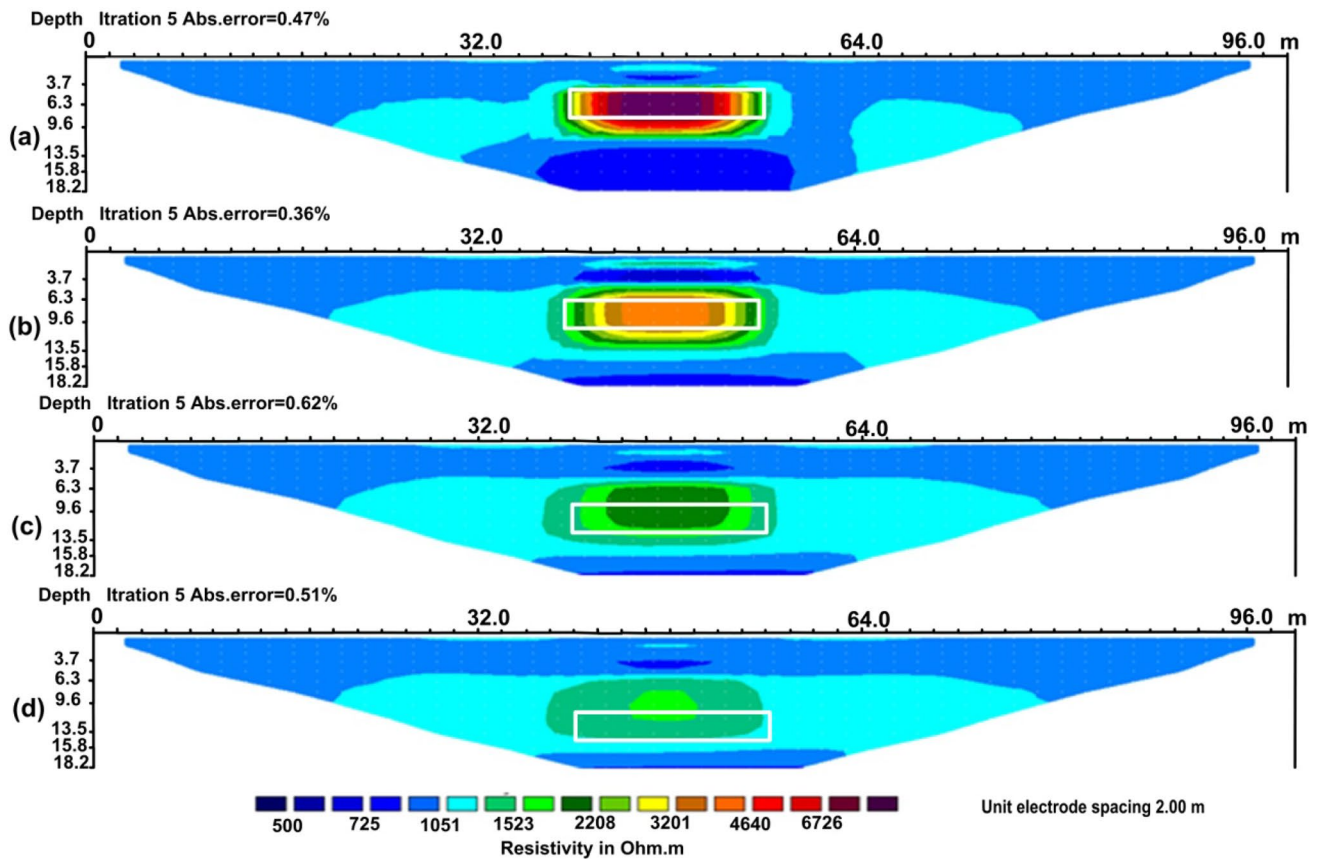
Fig. 6 The inverted resistivity models using WS array for the cavity models: **a** L1, **b** L2, **c** L3, **d** L4. The white boxes represent the actual position and dimensions of the modelled cavities

Table 3 Values of the inverted resistivity for synthetic cavity models using individual and mixed array

Models	True model resistivity (Ω m)	Inverted maximum resistivity values (Ω m)					
		DD	PD	WS	DD-WS	PD-WS	DD-PD
Cavity model (L1)	10,000	8097	8097	8097	8097	8097	8097
Cavity model (L2)	10,000	5586	5586	4640	8097	8097	5586
Cavity model (L3)	10,000	3853	3200	2208	6726	4640	4640
Cavity model (L4)	10,000	2658	2208	1523	4640	2658	2208

The inverted model of the deep cavity (L4) located at 10.5 m depth for the composite DD-WS datasets (Fig. 7d) shows a moderate resolution in regard to the actual cavity model. Although, it is still the best compared to other composite datasets (i.e. DD-PD, PD-WS) and the individual selected arrays. The inverted model of the composite DD-WS datasets (Fig. 7d) shows a maximum resistivity anomaly of about 4640 Ω m, while maximum resistivity values of about 2208 Ω m and 2658 Ω m were reconstructed by DD-PD and PD-WS composite datasets respectively. Furthermore, the composite DD-WS datasets inverted model (Fig. 7d) shows adequate correlation regards to the location of the cavity anomaly related to the actual model, where the upper boundary of the anomaly

shifted upward by 2 m and the lower boundary of the anomaly shifted downward by only 1 m.

The inverted models of the composite datasets of DD-PD (Fig. 8) show the lowest resolution image for the cavity models recovered since neither the shape nor the location was resolved well. On the other hand, the inverted models of the composite datasets of PD-WS (Fig. 9) show a moderate resolution in between the inverted models obtained by DD-WS and DD-PD. It is clear that the use of composite datasets of DD and WS arrays could give optimal information regarding cavity detection rather than using one single array or using composite datasets of DD-PD and PD-WS, since [39] had earlier mentioned that, the reliability of the resistivity image section obtained
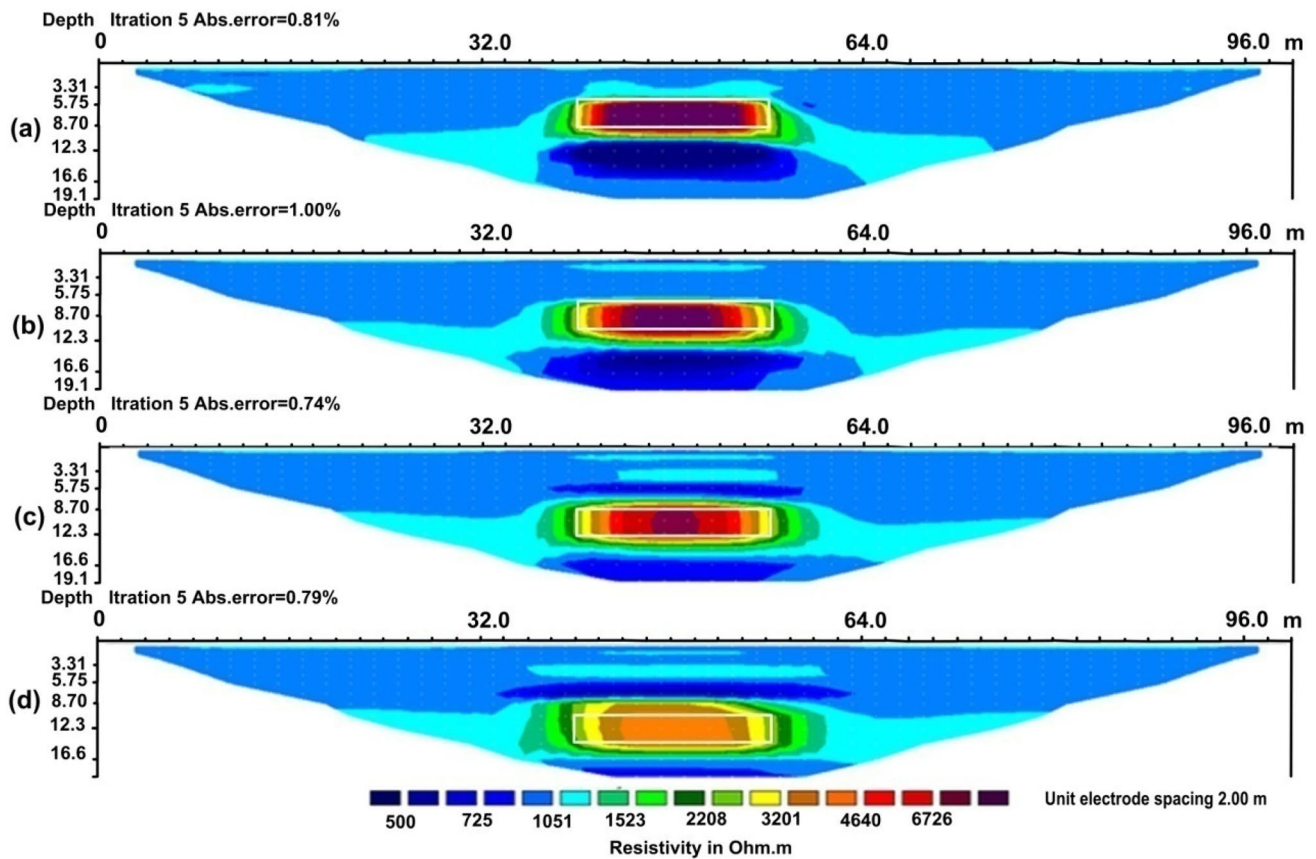
Fig. 7 The inverted resistivity models using composite datasets of DD-WS arrays for the cavity models: **a** L1, **b** L2, **c** L3, **d** L4. The white boxes represent the actual position and dimensions of the modelled cavities

by an array restricted by getting maximum anomaly information.

The model quality is usually related to the percentage error during the inversion process. However, an inverted model with a large error can give an accurate and realistic model than one with a small error [24, 26]. The present study corroborated the findings of [24, 26]. For example, the inverted resistivity section of the composite datasets of DD-WS for cavity model L4 produces higher Abs. error (Fig. 10) it shows the better model resolution among the other array. In contrast, the inverted resistivity section of the WS for cavity model L2 produces the lower Abs. error (Fig. 10) it shows the lower model resolution than other arrays.

4 Discussion

Accurate mapping of subsurface cavities using the ERT technique is still a challenging task in environmental studies [11, 12, 40]. One of the important factors that imaging subsurface cavities depends on using the ERT technique is the choice of an appropriate electrode array for

measurements. Many previous studies compared the ability of different individual electrode arrays for subsurface cavity detection [13, 25, 26]. Insight the finding results of the present study the DD array exhibits a better resolution than PD and WS for cavity detection, consistent with previous studies made by [25, 26].On the other hand, the WS array yields a lower resolution model than the other individual arrays, thus contradicting the field study carried out by [13]. Depending on the recovering ability of the model's cavity parameters including the resistivity and geometry, the DD array has the priority followed by the PD array while the WS array is the least effective one for cavity detection. The cavity depth is considered an important factor in cavity detection. Figures 4 and 5, and 6 show that, the accurate determination of cavity dimensions decrease as the cavity depth increase. The geometry of the cavity can be located until 6 m depth, which means that accurate detection of a cavity can be successful at depths equal to 3 times the half-width of the cavity.

The above-mention discussion illustrated the limitation of using the individual arrays in cavity detection. This limitation can be solved by using the mixed array datasets. Therefore, the mixed array reduces misinterpretation and
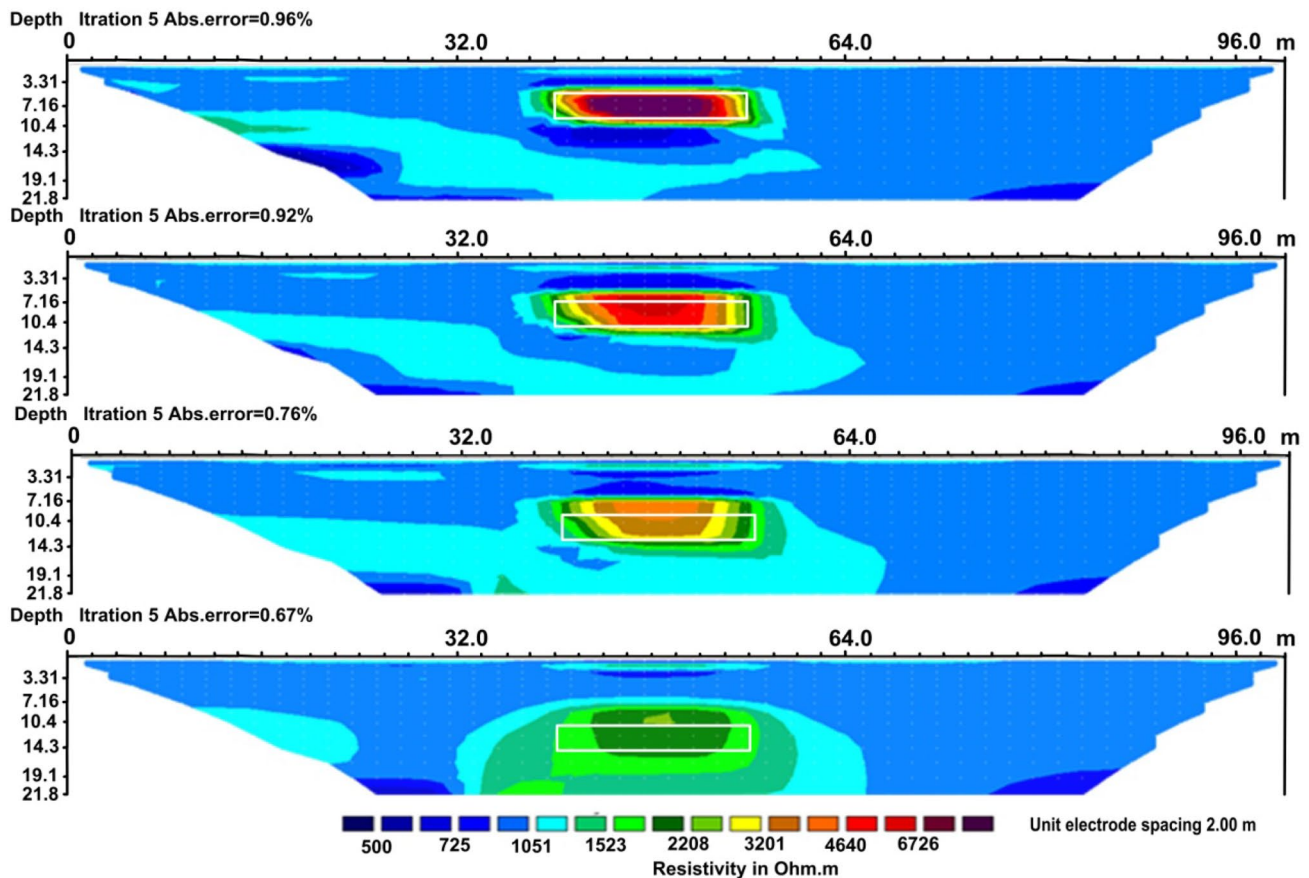
Fig. 8 The inverted resistivity models using composite datasets of DD-PD arrays for the cavity models: **a** L1, **b** L2, **c** L3, **d** L4. The white boxes represent the actual position and dimensions of the modelled cavities

increase the lateral and vertical resolution of the obtained model as well [19]. In general, the inverted resistivity sections for DD-WS (Fig. 7), DD-PD (Fig. 8), and PD-WS (Fig. 9) mixed arrays show a better resolution in model resistivity than that obtained by the individual array. The higher resolution stand behind using the mixed arrays is that the increase of the data points and data levels and thus, minimizes the interpolation yielding a more realistic resistivity model. This corroborated with the outcome of [40] that concluded that increasing the acquired data points using the ERT technique would delineate anomaly parameters (e.g. position, shape, resistivity values) more accurately after inversion. Moreover, the DD-WS mixed array has the best resolution among the other mixed array types, consistent with the findings of [32, 41]. The DD-WS mixed array can recover the cavity geometry until a 10 m depth below the surface is equal to 5 times the half-width of the cavity.

The outcome of this paper shows that the resolution of the subsurface geological structures (e.g. cavity) can be improved by using mixed datasets of two arrays. The composite datasets improve the vertical resolution of

the inverted sections by increasing the number of datum points as well as the number of data levels. This can significantly reduce the ambiguity and misinterpretation of the exponential decrease of resistivity resolution with depth. Also, the results of the present study illustrate the usefulness of the numerical modelling approach for testing the efficiency of resistivity images with different types of arrays and/or mixed arrays for resolving and obtaining optimal information about any subsurface structures before the actual field investigation.

5 Conclusions

Synthetic resistivity models were adopted to simulate subsurface cavities located at various depths in order to investigate the performance of composite datasets technique for cavity studies. The conceptual cavity models were simulated to calculate the potential difference of three common individual arrays namely DD, PD, and WS. Then the calculated potential difference of each pair of these arrays was merged to form a single composite dataset.
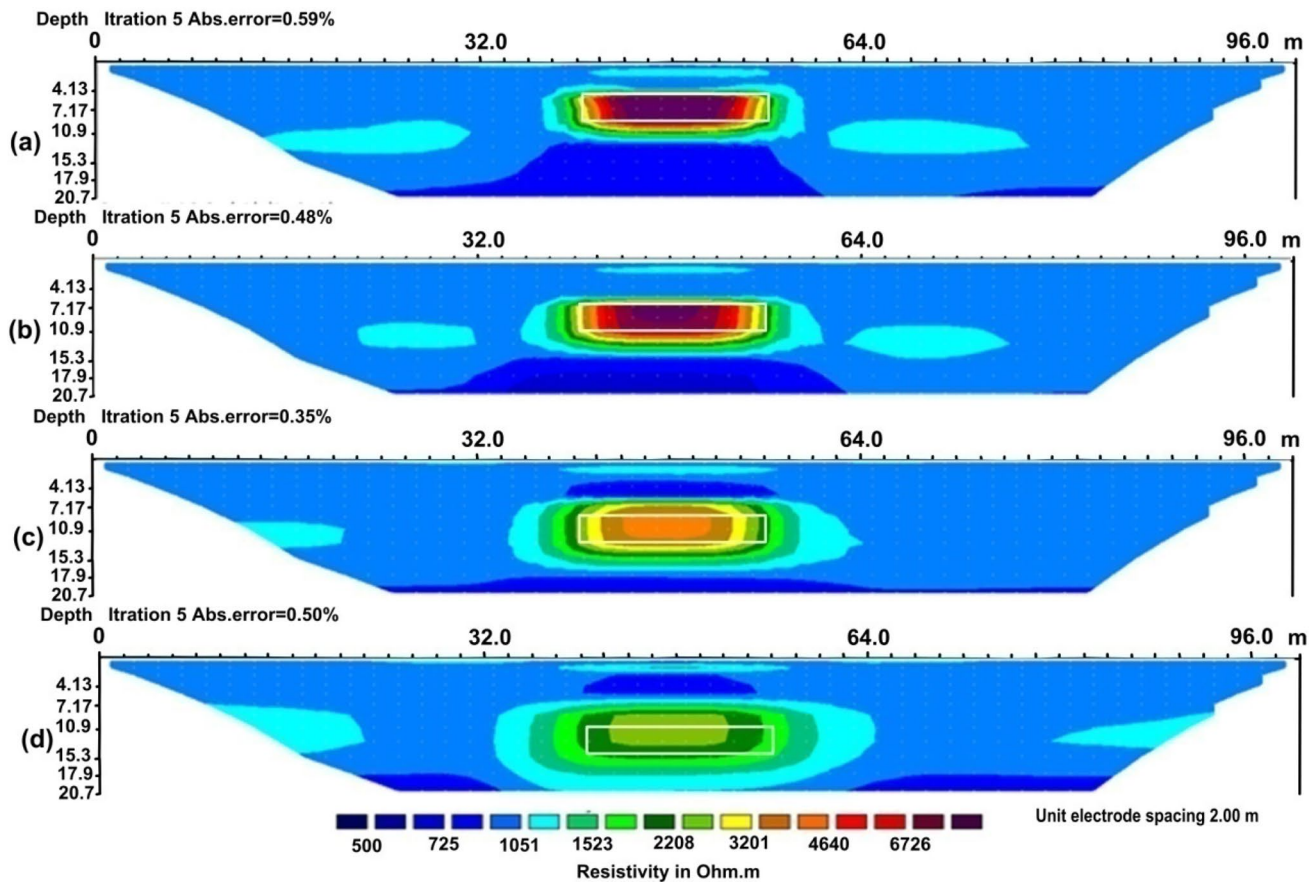
Fig. 9 The inverted resistivity models using composite datasets of PD-WS arrays for the cavity models: **a** L1, **b** L2, **c** L3, **d** L4. The white boxes represent the actual position and dimensions of the modelled cavities

As a result, three possible mixed arrays can be obtained DD-WS, DD-PD, and PD-WS. The apparent resistivity data of both the individual and mixed arrays were inverted to examine the recovering ability of each one. The inverted resistivity sections were evaluated based on the location, size, depth, and resistivity value compared with actual cavity model parameters.
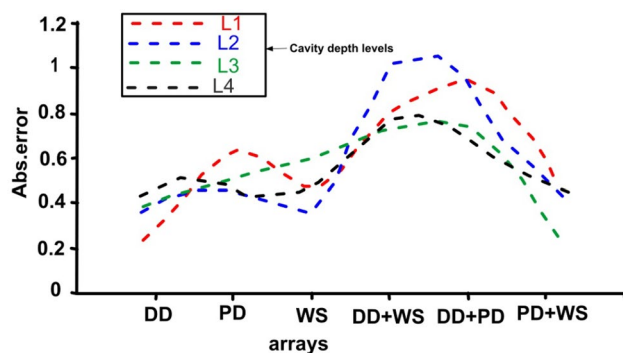
Fig. 10 Arrays' inversion error for different cavity depth levels

The inverted images of the synthetic resistivity models using the individual arrays (DD, PD, and WS) show their capability in cavity detection especially when the cavities were located at shallow depths, but the resolution and detectability decrease rapidly with increasing depth. The results show that the individual arrays exhibit accurate detection of the cavity model L1 (4.5 m depth) and L2 (6.5 m depth), on the other hand poor detection where observed when the cavity models were located at depths of 8.5 and 10.5 m.

In contrast, by using the composite datasets the resolution and detectability were improved and the reliability of the inverted image was increased. The composite datasets from dipole–dipole and Wenner–Shlumberger arrays are better than using mixed data from pole–dipole and Wenner–Shlumberger or dipole–dipole and pole–dipole arrays. The inverted resistivity section of DD-WS shows a good match of the cavity model parameters (e.g. actual location, size, and resistivity) even though the deeper location of the cavity (e.g. 8.5 and 10.5 m depth level). Subsequently, the mixed arrays of DD-WS can have the priority for imaging

cavities followed by the PD-WS mixed arrays as a second option.

This study demonstrated the usefulness of the composite datasets approaches in the enhancement of the resolution of the 2D resistivity image model regards cavity detection. So, this approach is recommended for cavity studies although the time and effort can be twice the reliability of the obtained results is better. Studying the response of mixed array datasets from more than two individual arrays is recommended as a future study.

Data availability The datasets generated during the current study are available from the corresponding author on reasonable request.

Declarations

References

1. Zhang G, Zhang GB, Chen CC, Chang PY, Wang TP, Yen HY, Dong JJ, Ni CF, Chen SC, Chen CW (2016) Imaging rainfall infiltration processes with the time-lapse electrical resistivity imaging method. Pure Appl Geophys 173:2227–2239. https://doi.org/10.1007/s00024-016-1251-x
2. Chang PY, Chang LC, Hsu SY, Tsai JP, Chen WF (2017) Estimating the hydrogeological parameters of an unconfined aquifer with the time-lapse resistivity-imaging method during pumping tests: case studies at the Pengtsuo and Dajou sites. Taiwan J Appl Geophy 144:134–143. https://doi.org/10.1016/j.jappgeo.2017.06.014
3. Paz MC, Alcala FJ, MedeirosA, Martinez-Pagan P, Perez-Cuevas J, Ribeiro L (2020) Integrated MASW and ERT Imaging for geological definition of an unconfined alluvial aquifer sustaining a coastal groundwater-dependent ecosystem in Southwest Portugal. Appl Sci 10(17):5905. https://doi.org/10.3390/app10175905
4. Rucker DF, Loke MH, Levitt MT, Noonan GE (2010) Electrical resistivity characterization of an industrial site using long electrodes. Geophysics 75:WA95–WA104. https://doi.org/10.1190/1.3464806
5. Abdulrahman A, Nawawi M, Saad R, Abu-Rizaiza AS, Yusoff MS, Khalil AE, Ishola KS (2016) Characterization of active and closed landfill sites using 2D resistivity/IP imaging: case studies in Penang, Malaysia. Environ Earth Sci 75(4):347. https://doi.org/10.1007/s12665-015-5003-5
6. Caputo R, Piscitelli S, Oliveto A, Rizzo E, Lapenna V (2003) The use of electrical resistivity tomographies in active tectonics:examples from the Tyrnavos Basin. Greece J Geodyn 36:19–35. https://doi.org/10.1016/S0264-3707(03)00036-X
7. Fazzito SY, Rapalini AE, Cortés JM, Terrizzano CM (2009) Characterization of quaternary faults by electric resistivity tomographyin the Andean Precordillera of Western Argentina. J S Am Earth Sci 28:217–228. https://doi.org/10.1016/j.jsames.2009.06.001
8. Hamad HA, Mohammed SF, Sattam AA, Mansour SA, Kamal A (2021) Electrical resistivity and refraction seismic tomography in the detection of near-surface Qadimah Fault in Thuwal-Rabigh area, Saudi Arabia. Arab J Geosci 14:1153. https://doi.org/10.1007/s12517-021-07524-2
9. Chang PY, Chen CC, Chang SK, Wang TB, Wang CY, Hsu SK (2012) An investigation into the debris flow induced by Typhoon Morakot in the Siaolin Area, Southern Taiwan, using the electrical resistivity imaging method. Geophys J in 188:1012–1024. https://doi.org/10.1111/j.1365-246X.2011.05310.x
10. Aal AE, Nabawy AK, Aqeel BS, Abidi A A (2020) Geohazards assessment of the karstified limestone cliffs for safe urban constructions, Sohag, West Nile Valley, Egypt. J Afr Earth Sci 161:1–11. https://doi.org/10.1016/j.jafrearsci.2019.103671
11. Van Schoor M (2002) Detection of sinkholes using 2D electrical resistivity imaging. J Appl Geophy 50:393–399. https://doi.org/10.1016/S0926-985
12. Cardarelli E, Cercato M, Cerreto A, Di Filippo G (2010) Electrical resistivity and seismic refraction tomography to detect buried cavities. Geophys Prospect 58(4):685–695. https://doi.org/10.1111/j.1365-2478.2009.00854.x
13. Martinez-Lòpez J, Rey J, Duenas J, Hidalgo C, Benavente J (2013) Electrical tomography applied to the detection of subsurface cavities. J Cave Karst Stud 75(1):28–37. https://doi.org/10.4311/2011ES0242
14. Szalai S, Szarka L (2008) On the classification of surface geoelectric arrays. Geophys Prospect 56:159–175. https://doi.org/10.1111/j.1365-2478.2007.00673.x
15. Telford WM, Geldart LP, Sheriff RE (1990) Applied geophysics, vol 1. Cambridge university press, Cambridge
16. Reynolds JM (2011) An introduction to applied and environmental geophysics. Wiley, New York
17. Everett ME (2013) Near-surface applied geophysics. Cambridge University Press, Cambridge
18. Loke MH (2012) Tutorial: 2-D and 3D Electrical Imaging Surveys. University of Alberta, Edmonton, p 165
19. Zhou W, Beck BF, Adams AL (2002) Effective electrode array in mapping karst hazards in electrical resistivity tomography. Environ Geol 42:922–928. https://doi.org/10.1007/s00254-002-0594-z

20. Satarugsa P, Nulay P, Meesawat N, Thongman W (2004) Applied two-dimension resistivity imaging for detection of subsurface cavities in Northeastern Thailand: a case study at Ban nonsa bang, Mphoe Ban muung, changwad Stakonnakhon. In: International conference on applied geophysics, 26–27, Chiang Mai, Thailand pp 187–202

21. Dahlin T, Zhou B (2004) Numerical comparison of 2D resistivity imaging with ten electrode arrays. Geophys Prospect 52:379–398. https://doi.org/10.1111/j.1365-2478.2004.00423.x

22. Reiser F, Dalsegg E, Dahlin T, Guri V, GanerØd, RØnning JS (2009) Resistivity modeling of fracture zones and horizontal layers in bedrock. Nor Geol Surv 2009.070:120

23. Olayinka A, Yaramanci U (2000) Assessment of the reliability of 2D inversion of apparent resistivity data. Geophys Prospect 48:293–316. https://doi.org/10.1046/j.1365-2478.2000.00173.x

24. Yang X, Lagmanson MB (2003) Planning resistivity surveys using numerical simulations. In Proceedings of the 16th EEGS Symposium on the Application of Geophysics to Engineering and Environmental Problems, San Antonio, TX, USA, 6–10 April 2003; p. cp-190-00047

25. Hassan AA (2017) Numerical modelling of subsurface cavities using 2D electrical resistivity tomography technique. Diyala J Pure Sci (DJPS) 13(2):197–216. https://doi.org/10.24237/djps.1302.260A

26. Doyoro YG, Chang PY, Puntu JM (2021) Uncertainty of the 2D resistivity survey on the subsurface cavities. Appl Sci 11:3143. https://doi.org/10.3390/app11073143

27. Loke MH (2004) Rapid 2-D Resistivity and IP inversion using the least-squares method. Geoelectrical Imaging 2D and 3D GEOTOMO Software, Malaysia, p 133

28. Oldenburg DW, Li Y (1999) Estimating depth of investigation in DC resistivity and IP surveys. Geophysics 64:403–416. https://doi.org/10.1190/1.1444545

29. Loke MH (2001) Tutorial: 2-D and 3-D electrical imaging surveys http://www.geoelectrical.com

30. Portniaguine O, Zhdanov MS (1999) Focusing geophysical inversion images. Geophysics 64:874–887. https://doi.org/10.1190/1.1444596

31. Bharti AK, Pal SK, Priam P, Kumar S, Srivastava S, Yadav P (2016) Subsurface cavity detection over Patherdih colliery, Jharia Coalfield, India using electrical resistivity tomography. Environ Earth Sci 75:443. https://doi.org/10.1007/s12665-015-5025-z

32. Rekapalli R, Kumar D, Sarma VS (2019) Resolution enhancement for geoelectrical layer interpretation of electrical resistivity model from composite dataset: implication from physical model studies. Curr Sci 116:1356–1362. https://doi.org/10.18520/cs/v116/i8/1356-136

33. Ibrahim IM, Tezkan B, Bergers R (2021) Integrated interpretation of magnetic and ERT Data to characterize a landfill in the North West of Cologne, Germany. Pure Appl Geophys 178:2127–2148. https://doi.org/10.1007/s00024-021-02750-x

34. Loke MH (2000) Electrical imaging surveys for environmental and engineering studies-A practical guide to 2-D and 3-D surveys, Geotomo Software, p 67

35. Loke MH (2016) RES2DMOD ver. 3.03.01: Rapid 2D resistivity forward modeling using the finite-difference and finite-element methods. Geotomo Software. Malaysia, p 25

36. Dey A, Morrison HF (1979) Resistivity modeling for arbitrarily shaped two-dimensional structures. Geophys Prospect 27:106–136

37. Edwards LS (1977) A modified pseudosection for resistivity and induced polarization. Geophysics 42:1020–1036

38. Loke MH, Acworth I, Dahlin T (2003) A comparison of smooth and blocky inversion methods in 2D electrical imaging surveys. Explor Geophys 34:182–187

39. Okpoli CC (2013) Sensitivity and resolution capacity of electrode configurations. Geophys J Int 2013:608037. https://doi.org/10.1155/2013/608037

40. Abu-Shariah MII (2009) Determination of cave geometry by using a geoelectrical resistivity inverse model. Eng Geol 105:239–244. https://doi.org/10.1016/j.enggeo

41. Bery AA, Saad R (2013) Merging data levels using two different arrays for high resolution resistivity tomography. Electron J Geotech Eng 18:5507–5514